HHS Public Access

Author manuscript

Hepatology. Author manuscript; available in PMC 2023 August 09.

Published in final edited form as:

Hepatology. 2023 July 01; 78(1): 243–257. doi:10.1097/HEP.0000000000000307.

p16 INK4A Drives Non-Alcoholic Fatty Liver Disease Phenotypes in High Fat Diet Fed Mice via Biliary E2F1/FOXO1/IGF-1 Signaling

Debjyoti Kundu[2], **Lindsey Kennedy**[1,2], **Tianhao Zhou**[2], **Burcin Ekser**[6], **Vik Meadows**[2,*], **Amelia Sybenga**[3], **Konstantina Kyritsi**[2], **Lixian Chen**[2], **Ludovica Ceci**[2,7], **Nan Wu**[2], **Chaodong Wu**[8], **Shannon Glaser**[4], **Guido Carpino**[7], **Paolo Onori**[7], **Eugenio Gaudio**[7], **Gianfranco Alpini**[1,2], **Heather Francis**[1,2]

[1]Department of Research, Richard L. Roudebush VA Medical Center

[2]Division of Gastroenterology and Hepatology, Department of Medicine, Indiana University School of Medicine Research

[3]UVM Health Network

[4]Texas A&M University School of Medicine.

[6]Department of Surgery, Indiana University School of Medicine, Indianapolis, Indiana, USA

[7]Department of Anatomical, Histological, Forensic Medicine and Orthopedics Sciences, Sapienza University of Rome, Rome, Italy

[8]Department of Nutrition, Texas A&M University, College Station, Texas

Abstract

Background and aim: Non-alcoholic fatty liver disease (NAFLD) is characterized by steatosis, hepatic inflammation, and fibrosis which can develop into non-alcoholic steatohepatitis (NASH). NAFLD/NASH patients have increased ductular reaction (DR) and biliary senescence. High fat/high cholesterol diet (HFD) feeding increases biliary senescence, DR, and biliary insulin-like growth factor-1 (IGF-1) expression in mice. p16/IGF-1 converges with fork-head box transcription

Address correspondence to: Heather Francis, Ph.D., FAASLD, Professor of Medicine, VA Research Career Scientist, Scientific Director, Indiana Center for Liver Research, Richard L. Roudebush VA Medical Center and Indiana University, Gastroenterology, Medicine, 702 Rotary Circle, Rm. 013C, Indianapolis, IN 46202, heafranc@iu.edu.

*Current address Department of Pharmacology and Toxicology, Rutgers University, New Brunswick, NJ

Author Contributions:

DK = substantial conceptual and design contributions, acquisition of data, analysis, and interpretation of data; generation of figures, drafting the article or revising it critically for important intellectual content; and final approval; LK = substantial contributions to acquisition of data and interpretation of data; revising the article critically for important intellectual content; and final approval; TZ = substantial contributions to acquisition of data and interpretation of data; revising article, and final approval; BE = substantial contributions to acquisition of data and interpretation of data; revising article, and final approval; VM = substantial contributions to acquisition of data and interpretation of data; revising article, and final approval; AS = substantial contributions to interpretation of data and final approval; KK = substantial contributions to acquisition of data; revising article, and final approval; LC = substantial contributions to acquisition of data; revising article, and final approval; LC = substantial contributions to acquisition of data; revising article, and final approval; NW = substantial contributions to acquisition of data; revising article, and final approval; CW = substantial contributions to interpretation of data; revising article, and final approval; SG = substantial contributions interpretation of data; revising article, funding/resources, and final approval GC = substantial contributions to acquisition of data and interpretation of data; revising article, and final approval; PO = substantial contributions to acquisition of data and interpretation of data; revising article, and final approval; EG = substantial contributions to acquisition of data and interpretation of data; revising article, and final approval; GA = substantial conceptual and design contributions, and interpretation of data; revising it critically for important intellectual content; funding/resources and final approval; HF = substantial conceptual and design contributions, data analysis and interpretation of data; drafting the article and revising it critically for important intellectual content; funding/resources and final approval

factor O1 (FOXO1) via E2F1. We evaluated p16 inhibition on NAFLD phenotypes and biliary E2F1/FOXO1/IGF-1 signaling. Approach: 4 wk wild-type (WT, C57BL/6J) male mice were fed control diet (CD) or HFD and received either p16 or control Vivo Morpholino (VM) by tail vein injection 2x during the 16th wk of feeding. We confirmed p16 knockdown and examined (i) NAFLD phenotypes; (ii) DR and biliary senescence; (iii) serum metabolites; and (iv) biliary E2F1/FOXO1/IGF-1 signaling. Human normal, NAFLD, and NASH liver samples and isolated cholangiocytes treated with control or p16 VM, were evaluated for p16/E2F1/FOXO1/IGF-1 signaling.

Results: p16 VM treatment reduced cholangiocyte and hepatocyte p16. In WT HFD mice with control VM, there was increased (i) NAFLD phenotypes, (ii) DR and biliary senescence, (iii) serum metabolites, and (iv) biliary E2F1/FOXO1/IGF-1 signaling; however, p16 VM treatment reduced these parameters. Biliary E2F1/FOX-O1/IGF-1 signaling increased in human NAFLD/NASH but was blocked by p16 VM. *In vitro*, p16 VM reduced biliary *E2f1* and *Foxo1* transcription by inhibiting RNA pol II binding and E2F1 binding at the *Foxo1* locus, respectively. Inhibition of E2F1 reduced biliary FOXO1, *in vitro.*

Conclusion: Attenuating hepatic p16 expression may be a therapeutic approach for improving NAFLD/NASH phenotypes.

Keywords

NASH; ductular reaction; inflammation; senescence; metabolites

---

Non-alcoholic fatty liver disease (NAFLD) and its advanced form, non-alcoholic steatohepatitis (NASH) have become a metabolic pandemic. Advancement of NAFLD to NASH is a principal risk factor for hepatocellular carcinoma development in various populations (1). In a recent study among NAFLD patients, 71.1% had NAFLD/NASH which encompasses hepatocyte ballooning and lobular inflammation and 29.8% of the total population assessed had NAFLD-associated cirrhosis (2).

Previous research substantiates the critical role of hepatocytes in NAFLD progression (3). During NAFLD/NASH progression, fat accumulation increases and hepatocyte cyclin dependent kinase inhibitor 2A ($p16^{INK4A}$) gene expression is upregulated (4). Following injury, cholangiocytes and biliary epithelial cells elicit a dynamic response as demonstrated by enhanced hyperplasia and portal inflammation resulting in ductular reaction (DR) (5). Cholangiocytes acquire a senescence-associated secretory phenotype (SASP) contributing to damage in primary sclerosing cholangitis (PSC) (6) and studies demonstrate that increased DR and biliary senescence contributes to damaging NAFLD phenotypes. Secretin/secretin receptor activation induces hepatocyte steatosis via cholangiocyte-derived microRNA (miR)-125b (7). Expression of insulin-like growth factor 1 (IGF-1) increases in cholangiocytes during NAFLD, recruiting mast cells (MCs) to the periportal region which promotes microvesicular steatosis (8).

NAFLD and end-stage NASH patients have increased expression of cyclin dependent kinase inhibitor 2A (CDKN2A or $p16^{INK4A}$) [i.e., p16]) (9). In PSC patients, p16 is positively

correlated with biliary SASP expression and knockdown of p16 in multi-drug resistant gene 2 knockout mice (*Mdr2*$^{-/-}$) alleviated SASP factors and reduced fibrosis (8).

Fork-head box transcription factor O1 (FOXO1) regulates cholangiopathic phentoypes (10). FOXO1 nuclear translocation is elevated in *Mdr2*$^{-/-}$ mice, which was reduced by ghrelin (10). FOXO1 promotes autophagy and lipogenesis via S100A11/HDAC6/FOXO1 signaling in NAFLD (11) and elevates hepatic very low-density lipoprotein production (12). Although FOXO1 has been studied within the context of hepatocyte function (3), the role of cholangiocyte FOXO1 and cellular senescence during NAFLD/NASH is not well understood. We explored the effects and signaling mechanisms of p16 inhibition in a murine model of NAFLD.

Materials and Methods

Unless otherwise specified, all materials were purchased from Sigma Aldrich (St. Louis, MO). Details for methods are provided in Supplemental Methods. Primer information is listed in Supplemental Table 1, and antibody information in Supplemental Table 2.

In Vivo Model

Approval for animal procedures was obtained from Indiana University School of Medicine (IUSM) Institutional Animal Care and Use Committee. Male wild-type (WT, C57BL/6J) mice were purchased from Jackson Laboratory (Bar Harbor, ME) at age 4 weeks and allowed to acclimate for 3 days prior to beginning feeding. Mice were pair-housed in temperature-controlled cages with 12:12 light: dark cycles and fed *ad libitum* with free access to drinking water and specific diets. Selected mice were fed a high fat diet (HFD) or control diet (CD) purchased from ENVIGO Diet Inc. (Indianapolis, IN) and fed as published (7, 13). Mice were fed with CD or HFD for 16 weeks and, during the last week of feeding, p16 or control Vivo Morpholinos (VMs) purchased from GeneTools LLC. (Philomath, OR) were administered via tail vein (12.5 mg/kg/BW dissolved in sterile water) on the first and fourth days (8).

Human Samples

Human liver tissues were collected from patients diagnosed with NAFLD or NASH and non-diseased controls by Dr. Burcin Ekser at IUSM or purchased from Sekisui XenoTech, LLC (Kansas City, KS). Explant tissues were obtained at transplant, and the diagnosis of NAFLD or NASH was determined by clinical, imaging, and pathological analyses. Written informed consent was obtained from each patient, and the study protocol conformed to the ethical guidelines of the 1975 Declaration of Helsinki as reflected in prior approval by the IUSM Institutional Review Board (no donor organs were obtained from executed prisoners or other institutionalized persons). De-identified patient information is provided in Supplemental Table 3.

p16 Expression

p16 immunofluorescence was performed co-stained with either cytokeratin-19 (CK-19, to evaluate bile duct expression) or hepatocyte nuclear factor 4 alpha (HNF4α, to identify

hepatocytes). Western blot for p16 expression was performed with 30 μg of isolated protein from total liver tissue. Total liver β-actin was used as a housekeeping control for the expression of p16. p16/CK-19/HNF4α immunofluorescence was performed to detect p16 expression in human normal, NAFLD and NASH liver sections.

Liver Damage and Hepatic Steatosis

Liver damage was assessed by hematoxylin and eosin (H&E) staining and serum chemistry. Fat deposition was evaluated by Oil Red O staining in liver sections using a kit from Abcam (Cambridge, UK) and was quantified using Image-Pro® software (Media Cybernetics, Rockville, MD) (13). We also used 4,4-difluoro-1,3,5,7,8-pentamethyl-4-bora-3a,4a-diaza-s-indacene (BODIPY) lipid stain from Thermo Fisher Scientific (Waltham, MA).

Hepatic lipid uptake and oxidation were evaluated by *q*PCR in total RNA isolated from hepatocytes in all mice for carnitine palmitoyl transferase 1a (*Cpt1a*), carnitine palmitoyl transferase 1b (*Cpt1b*), and fatty acid binding protein 1 (*Fabp1*) (14, 15) and immunoreactivity of FABP1 was evaluated in liver sections co-stained with CK-19 and HNF4α. Hepatocyte gene expression of glycerol-3-phosphate acyltransferase (*Gpat3*) and diacylglycerol acyl transferase 2 (*Dgat2*), related to *de novo* triglyceride biosynthesis was analyzed by *q*PCR in all mice.

Intrahepatic Bile Duct Mass (IBDM), Cellular Proliferation, Apoptosis, Hepatic Inflammation and MC Infiltration/Activation.

The effect of p16 VM on IBDM was assessed by immunohistochemistry for CK-19 and quantified using 3–4 images per tissue sectioned from at least 4 different animals per treatment group (16). Hepatic proliferation was assessed by immunohistochemistry for Ki-67 (16). Apoptosis was measured by terminal deoxynucleotidyl transferase dUTP nick end labeling (TUNEL) staining performed by using the *in situ* cell death detection kit, POD (SKU 11684817910). Hepatocyte and cholangiocyte TUNEL positive staining was quantified separately.

Liver inflammation was evaluated by staining for a cluster of differentiation 68 (CD-68) along with semi-quantification. Since (i) MCs promote hepatic steatosis and DR in NAFLD and (ii) WT mice fed HFD have increased MCs in the liver (13), we determined MC presence by immunohistochemistry for tryptase beta 2 (TPSβ2) in all mice (17). In total liver, we measured FC epsilon receptor 1 gamma (FCεR1γ) expression by *q*PCR to detect MC activation.

Hepatic Senescence, SASP, Fibrosis, and HSC Activation

Senescence was evaluated by immunofluorescence for cyclin dependent kinase inhibitor 2C (*Cdkn2c*, p18) co-stained with CK-19. By immunofluorescence, we triple stained liver sections for phosphorylated histone 2A (γH2A.X) (18), HNF4α and CK-19 to evaluate DNA damage in both hepatocytes and cholangiocytes, respectively. In pure cholangiocytes, *Cdkn2c* gene expression was measured by *q*PCR in all groups.

Hepatic fibrosis and collagen deposition was evaluated by Sirius Red staining and immunofluorescence was performed with desmin (co-stained with CK-19) to detect HSC activation (19).

Metabolomic Assessment

NAFLD/NASH generates a metabolic burden in humans and serves as a non-invasive biomarker for diagnosis (20). To analyze changes in serum metabolites, we used a tandem mass spectrometry-based approach and comprehensively analyzed over 200 lipid species using Biocrates MxP® Quant 500 Kit (Product number 21094.12) from Biocrates (Innsbruck, Austria). The relative levels of serum metabolites in n=4 mice/group were analyzed, and a heat map was generated using GraphPad® Prism 9.

E2F1/FOXO1/IGF-1 Signaling

By Ingenuity Pathway Analysis (IPA, Qiagen, Waltham, MA), we found a link between p16 and E2 promoter binding transcription factor 1 (E2F1)/FOXO1/IGF-1 and since both FOXO1 and IGF-1 have been implicated in NAFLD/NASH (21–23), we measured *E2F1* in total liver and isolated cholangiocytes and *FOXO1* and *IGF-1* in isolated cholangiocytes by *q*PCR. We measured FOXO1 immunoreactivity (co-stained with CK-19) in liver sections from all mice and in human normal, NAFLD and NASH liver samples. Isolated cholangiocytes were collected from normal, NAFLD and NASH livers (n=1/group) and immortalized (see Supplemental Methods) prior to being treated with either 6μM of p16 (5'CCGGCTCCATGCTGTCCCC3') or control (5′-CCTCTTACCTCAGTTACAA TTTATA3') VMs (dissolved in sterile water). Human control and p16 VMs were tagged with fluorescein isothiocyanate (FITC) to assess VM internalization and immunofluorescent staining performed for p16/FITC (to assess knockdown viability), FOXO1 and IGF-1. In isolated normal (control), NAFLD and NASH cholangiocytes treated with either human control or p16 VM and *E2F1* and *IGF-1* gene expression measured by *q*PCR.

To evaluate the effect of p16 VM on E2F1 mRNA stability *in vitro,* we performed RNA-half-life analysis following actinomycin D-mediated global transcriptional blocking. Transcriptional activity of *E2f1* locus under p16 VM treatment was evaluated by Chromatin-immunoprecipitation (ChIP) of RNA pol II (Rpb1 NTD) followed by PCR for *E2f1*. To demonstrate that E2F1 directly regulates FOXO1 expression, an immortalized murine cholangiocyte line (IMCL) was treated with an E2F1 antagonist (HLM006474, 30 μM and 35 μM for 24hrs) or 0.1% DMSO (vehicle) and FOXO1 immunoreactivity was assessed. *In vitro*, to evaluate the binding of E2F1 transcription factor to *Foxo1* promoter region, IMCLs were treated with FFAs and we performed ChIP for E2F1 followed by *q*PCR for *Foxo1*. We evaluated E2F1 degradation *in vitro* by co-immunoprecipitation (co-IP) of total and ubiquitinated E2F1in IMCLs under FFA treatment; in the presence and absence of p16 VM.

Statistical Analysis

Data are represented as mean ± standard error of the mean (S.E.M). Statistical differences between groups were analyzed by the Student's unpaired t-test when two groups were analyzed and by one-way ANOVA when more than two groups were analyzed, followed by

the appropriate posthoc test. Heatmaps and box and whisker plots were made using Prism (GraphPad® version 9.0). $P<0.05$ was considered significant. Further methodological details are provided in Supplemental Methods.

Results

p16 Expression Increases in WT Mice Fed HFD and Human NAFLD/NASH; VM Treatment Reduces Hepatic p16 Expression in Mice

Cholangiocyte and hepatocyte p16 expression increased in WT HFD control VM mice compared to WT CD control VM, which was reduced in WT HFD p16 VM mice (Figure 1A–B). By Western blot (n=1), p16 protein expression increased in total liver from WT HFD compared to CD fed mice treated with control VM, and p16 VM injection reduced the expression of p16 in the total liver of WT HFD mice (Supplemental Figure 1A). In human NAFLD/NASH, p16 immunoreactivity was upregulated in both cholangiocytes and hepatocytes compared to normal (Figure 1C).

p16 VM Decreases Liver Damage, Lipid Deposition, Triglyceride Biosynthesis and Hepatocyte Lipid Uptake and Transport in WT HFD Mice

Liver weight (LW) significantly increased in WT HFD control VM mice compared to CD control VM group, which decreased in WT HFD p16 VM mice; however, no statistical differences were found in mean body weight (BW) between these groups. WT HFD control VM mice had increased LW/BW ratio compared to CD control VM mice, which decreased in WT HFD p16 VM mice (Table 1). ALT and AST levels (Table 2) and total serum cholesterol (Table 2) increased in WT HFD control VM mice, which were significantly reduced in WT HFD p16 VM mice.

WT HFD mice had moderate steatosis with ballooning hepatocytes and inflammation compared to CD control VM mice. WT HFD p16 VM mice displayed reduced steatosis, and the absence of ballooning hepatocytes (Figure 2A). WT HFD control VM mice had significantly higher lipid droplet presence compared to WT CD control VM; however, WT HFD p16 VM mice showed a significant reduction in lipid droplet presence compared to control VM (Figure 2B). WT HFD control VM mice had enhanced neutral lipid staining characterized by enlarged fat droplet accumulation compared to WT CD control VM mice (Figure 2C) that was reduced in WT HFD p16 VM mice (Figure 2C). Hepatocyte gene expression of *Gpat3, and Dgat2* increased in WT HFD control VM compared to WT CD control VM mice and p16 VM decreased these genes compared to WT HFD control VM mice (Supplemental Figure 1B).

Hepatocyte *Cpt1a, Cpt1b,* and *Fabp1* increased in WT HFD control VM mice, but WT HFD p16 VM mice showed a significant decrease in these genes compared to WT HFD control VM mice (Figure 3A). Hepatocyte and cholangiocyte immunoreactivity of FABP1 increased in WT HFD control VM mice, which decreased in WT HFD p16 VM mice (Figure 3B).

Blocking p16 Reduces IBDM, Cellular Proliferation, Senescence and Apoptosis in HFD Mice

IBDM increased in WT HFD control VM treated mice; however, in WT HFD p16 VM mice IBDM decreased (Supplemental Figure 2A). Similarly, WT HFD control VM mice had increased hepatic proliferation compared to controls that decreased WT HFD p16 VM mice (Supplemental Figure 2B). Apoptosis significantly increased in both cholangiocytes and hepatocytes in WT HFD control VM mice compared to the WT CD control VM group. In WT HFD p16 VM mice, apoptosis decreased in both cell types compared to the WT HFD control VM mice (Supplemental Figure 2C).

Hepatocye and cholangiocyte γH2A.X immunoreactivity increased in WT HFD control VM mice compared to WT CD control VM mice, which was reduced in WT HFD p16 VM mice (Figure 4A). Moreover, p18/CK-19/HNF4α increased demonstrating elevated senescence in cholangiocytes and hepatocytes in WT HFD control VM mice; however, this decreased in WT HFD p16 VM compared to WT HFD control VM mice (Figure 4B). Cholangiocyte *p18 (Cdkn2c)* expression was unchanged in WT HFD control VM mice compared to WT CD control or p16 VM mice, but significantly decreased in WT HFD p16 VM mice (Figure 4C).

p16 VM Treatment Decreases Hepatic Fibrosis, HSC Activation, Inflammation and MC Infiltration in WT Mice Fed HFD

WT HFD control VM mice display increased collagen deposition (Figure 5A), desmin immunoreactivity (Figure 5B) and CD-68^{+} cells (24) (Figure 5C) compared to WT CD control VM mice, all of which decreased in WT HFD p16 VM mice.

Fcer1g gene expression increased in WT HFD mice treated with control VM compared to CD which significantly decreased when WT HFD mice were treated with p16 VM (Supplemental Figure 1C). MC presence increased in the portal area of WT HFD mice treated with control VM and in WT HFD p16 VM mice, MC presence decreased (Supplemental Figure 1D).

Knockdown of p16 Reduces Serum Metabolites in WT HFD-Fed Mice

Heatmaps generated from Biocrates Q500 assay demonstrated multiple changes in circulating lipid species including ceramides (Cer) (Supplemental Figure 3A), acylcarnitines, Kynurenine and OH-GluAcid (3-hydroxyglutaric acid) (Supplemental Figure 3B). Cer(d18:1/18:1) but not Cer(d18:1/18:0) (Supplemental Figure 3C–D) were significantly upregulated in serum from WT HFD control VM mice compared to CD control VM mice and in WT HFD p16 VM mice, both parameters significantly decreased. Acylcarnitine C14:1 or tetradecenoylcarnitine (Supplemental Figure 3E) did not change between CD and WT HFD control VM mice; however, C18:1 or octadecenoylcarnitine (Supplemental Figure 3F) was significantly upregulated in serum from WT HFD control VM compared to CD control VM mice. In WT HFD p16 VM mice, C14:1 and C18:1 significantly decreased compared to controls. Kynurenine, a tryptophan metabolite increased in the serum of WT HFD control VM mice and significantly decreased with p16 VM treatment (Supplemental Figure 3G). There was no significant increase in OH-GluAcid

serum content from WT HFD control VM mice compared to CD control VM mice; however, in WT HFD p16 VM mice, OH-GluAcid significantly decreased (Supplemental Figure 3H).

p16 Regulates NAFLD/NASH via Biliary E2F1/FOXO1/IGF-1 Signaling

In isolated human NAFLD cholangiocytes, control VM (green, top panel) co-localized (magenta) with p16 (red) within the cytoplasm and nuclei but did not reduce p16 expression. In NAFLD cholangiocytes treated with p16 VM, p16 immunoreactivity decreased (Supplemental Figure 4A). *In vitro* treatment with p16 VM decreased p16 IMCL immunoreactivity (Supplemental Figure 4B). IMCLs treated with p16 VM or control VM plus FFA treatment had decreased p16 immunoreactivity compared to controls. p16 VM significantly reduced p16 expression in SA and PA (but not OA) treated IMCLs compared to IMCLs treated with FFAs alone (Supplemental Figure 4C).

We used IPA to elucidate the relationship between p16 and IGF-1 (*Igf1*) via the E2F1/FOXO1 axis (Supplemental Figure 5A). IGF-1/IGF-1R is a canonical downstream target of FOXO1 implicated in cholangiopathies (12). Biliary FOXO1 immunoreactivity increased in WT HFD control VM mice and, in WT HFD p16 VM mice, FOXO1 immunoreactivity decreased (Figure 6A). In human NAFLD/NASH liver samples, biliary FOXO1 immunoreactivity increased compared to normal (Figure 6B). By *q*PCR we found reduced *E2f1* expression in both total liver (Supplemental Figure 5B) and isolated cholangiocytes (Supplemental Figure 5C) from WT HFD p16 VM compared to WT HFD control VM mice. In isolated cholangiocytes, the gene expression of *Foxo1* (Supplemental Figure 5D) and *Igf1* (Supplemental Figure 5E) increased in WT HFD mice compared to CD control VM and, in WT HFD p16 VM mice, *Foxo1* and *Igf1* decreased (Supplemental Figure 5D and 5E). Isolated human cholangiocytes from NAFLD and NASH patient livers had increased p16 immunoreactivity (Figure 7A), FOXO1 (Figure 7B) and IGF-1 (Figure 7C) compared to normal that were reduced by p16 VM. Finally, isolated cholangiocytes from NAFLD and NASH patients had increased *E2F1* (Supplemental Figure 5F), and *IGF-1* (Supplemental Figure 5G) expression compared to control and, when NAFLD or NASH cholangiocytes were treated with p16 VM, *E2F1* expression decreased; however, only NASH cholangiocytes treated with p16 VM had decreased *IGF-1* expression compared to healthy control.

To further assess p16→E2F1→FOXO1 signaling, we performed ChIP for RNA pol II (Rpb1 NTD) and E2F1 separately, followed by *q*PCR for *E2f1* and *Foxo1*. p16 VM treatment reduced RNA pol II binding the E*2f1* promoter region compared to OA treatment alone (Supplemental Figure 6A). We found that p16 VM reduced E2F1 binding to *Foxo1* promoter region in IMCLs treated with OA compared to OA treatment alone (Supplemental Figure 6B).

We found that E2F1 transcript half-life was not significantly reduced with p16 VM treatment compared to FFA treatment (Supplemental Figure 6C); however, inhibition of E2F1 significantly reduced IMCL FOXO1 immunoreactivity compared to vehicle (0.1% DMSO) and basal (no treatment) controls (Supplemental Figure 6D). We performed co-IP and pulled down E2F1 from whole cell lysates and probed for total E2F1 (Supplemental

Figure 6E) and ubiquitinated-E2F1 (Supplemental Figure 6F). *In vitro*, p16 VM did not alter total or ubiquitinated E2F1 protein levels compared to the FFA treatment alone.

Finally, we analyzed whether p16 VM injection affected the gene expression of cyclin dependent kinase 4 (*Cdk4)* and cyclin D1 (*Ccnd1*), a cell cycle-promoting complex regulated by p16. *Cdk4* expression was unchanged in CD control and p16 VM treatment and in WT HFD control VM treatment; however, in WT HFD p16 VM mice, *Cdk4* expression significantly increased compared to control VM (Supplemental Figure 7A). *Ccnd1* was significantly decreased in CD p16 VM mice and HFD control VM mice compared to WT CD control VM. In WT HFD p16 VM mice, *Ccnd1* expression increased compared to HFD control VM (Supplemental Figure 7B).

Discussion

p16-regulated biliary and hepatocyte senescence plays a critical role in the progression of NAFLD/NASH mediated by biliary E2F1/FOXO1/IGF-1 signaling in both a mouse model of NAFLD and human NAFLD and NASH samples (Figure 8). NASH primarily targets hepatocytes; however, studies show that cholangiocytes contribute to hepatic steatosis and eventual scarring and fibrosis (7, 13). Cholangiocyte damage manifests as cellular senescence characterized by increased SASP which induces inflammation (5, 8). Many factors are involved in NAFLD/NASH progression, making it challenging to determine a single pathway that contributes to the disease within the context of cellular senescence.

p16 expression increases in rats fed HFD for 9 wks (4) and we also found enhanced hepatocyte and cholangiocyte p16 in WT HFD mice and in human NAFLD/NASH patients. Further, we identified increased p16 immunoreactivity in human cholangiocytes isolated from fresh NAFLD and NASH samples. p21 may also play a role in NAFLD; however, contrary to p16, hepatic p21 expression decreases in HFD-fed models (4). p16 expression increases in human PSC and mouse models of cholestatic injury (6, 25), and studies demonstrate that increased senescence may indicate worsening pathogenesis (26).

p16 VM inhibits PSC phenotypes in *Mdr2*$^{-/-}$ mice by miR-34a/sirtuin 1 signaling (8). We found that p16 VM significantly reduced NAFLD phenotypes; however, contrary to our findings, *p16*$^{-/-}$ mice fed methionine-choline deficient (MCD) diet displayed exacerbated steatosis and liver damage compared to controls (27). There are several factors to explain these contradictory findings. In the study the authors used a whole-body *p16*$^{-/-}$ which may have induced off-target effects in other cells, tissues, and organs (27). In contrast, we acutely knocked-down p16 thereby manipulating cellular senescence without potentially driving cells into cell cycle stress or mitochondrial dysfunction. Further, the authors (27) used MCD diet, which is a notable toxic model, whereas we used a milder “Western Diet” model. These studies highlight the careful balance that must be maintained when manipulating cellular senescence as these genes play critical roles in maintaining proper cell cycle progression.

Cellular senescence may promote fat accumulation (28) suggesting a feedback mechanism whereby exacerbated cellular p16 contributes to active lipid uptake. Our data support this since inhibition of p16 during the final week of HFD feeding resulted in decreased FABP1

and serum metabolites. Fat accumulation may occur in cells subjected to irreversible cell-cycle arrest which are unable to mitigate the generation of reactive oxygen species thus releasing a wide array of proinflammatory factors or SASPs (29). Studies demonstrate that exposure to HFD increases biliary SASP components such as TGF-β1 (7) along with IGF-1, fibroblast growth factor and IL-6 (13). Increased biliary SASP may drive elevated IBDM during NAFLD, which may begin as a compensatory mechanism to repair the liver during HFD-induced damage but, if left unchecked, contributes to hepatic fibrosis and inflammation (5). We observed increased DR in WT HFD mice whereas inhibition of p16 during the last week of feeding decreased IBDM. While cholangiocytes may not be the main target of NAFLD, biliary senescence/SASP induces a paracrine interaction between cholangiocytes and hepatocytes that drive NAFLD phenotypes.

Blocking biliary secretin signaling (7) or MC infiltration/activation (13) in mice subjected to HFD, reduces biliary senescence, hepatic fibrosis, HSC activation and inflammation which is in accordance with our study. However, CCl_4 treated-BALB/c $p16^{-/-}$ mice had increased collagen deposition and HSC activation, directly opposing our findings (30). One difference in our model versus the $p16^{-/-}$ model is that the latter induces continual inhibition of p16, whereas in our study, p16 expression is induced by HFD and subsequently inhibited by VM during peak senescence rather than chronic knockdown. Using p16 VM, we reduced hepatic fibrosis and HSC activation presumably through cholangiocyte-HSC crosstalk. Supporting this, both p16 and p21 are increased in bile duct cells during stage 3 and 4 fibrosis of NAFLD/NASH patients, that also expressed CC motif chemokine ligand 2, which can serve as a chemoattractant for activated HSCs within septal fibrosis promoting portal inflammation (31). In pediatric NAFLD, DR significantly correlated to fibrosis and NASH progression (32) and, in a cohort of patients with a specific genetic mutation in patatin-like phospholipase domain containing 3, both hepatic stem- and hepatic progenitor cell (HPC) activation increased along with extensive fibrosis that positively correlated to DR (33). Our studies also demonstrate the potential crosstalk between DR/cholangiocytes and inflammation/macrophages as we show that decreased DR coincides with decreased inflammation. In support of this, it has been demonstrated that macrophage polarization induced changes in HPC phenotype during NAFLD/NASH (34) and, in obese patients, macrophage presence, steatosis and HSC activation correlated with proinflammatory cytokines (35) suggesting a cascade of multi-cellular interactions promoting NAFLD/NASH.

Fatty liver and senescence are regulated by caloric intake and WT mice subjected to *ad libitum* chow feeding versus a restricted diet for 9 months had increased cellular senescence as indicated by enhanced γH2A.X staining and telomere shortening (28). Upon clearance of senescence using either a transgenic mouse model or with senolytic therapy, NAFLD phenotypes were ameliorated (28). Interestingly, there were no significant changes in BW between WT HFD control or p16 VM mice, which may be due to the exacerbation of excessive fat and “sugar” content compared to *ad libitum* feeding; however, p16 VM markedly reduced cellular senescence in WT HFD mice.

Serum metabolites are a non-invasive tool of choice for diagnosing NAFLD and metabolites from serum lipidome of various patient cohort studies have been identified as potential NAFLD biomarkers (36). In accordance with previous studies (37–39), we identified several

upregulated acylcarnitines in serum from WT HFD mice that were decreased with p16 VM injection indicating an overall improvement of the metabolic profile (37). Kynurenine and 3-hydroxyglutaric acid are elevated in NAFLD patients and indicate mitochondrial stress, apoptosis, and pro-oxidation (40), and kynurenine increases inflammation via arachidonic acid in NASH patients (38). Interestingly, kynurenine is upregulated in patients with mastocytosis (41) suggesting a link between kynurenine and MC activation. We found an increase in MC infiltration and in support of this, in cirrhotic patients, histamine and kynurenine levels positively correlate (39). Since this metabolite is also linked to inflammation, which we found to be mediated by p16, we speculate that biliary senescence, kynurenine and MCs may interact synergistically during NAFLD/NASH progression.

We identified FOXO1 as a transcriptional activator in NAFLD-associated senescent damage. FOXO1 expression increases in steatohepatitis and correlates with enhanced liver fibrosis (42). Hepatocyte and cholangiocyte FOXO1 immunoreactivity increased in WT HFD mice and human NAFLD/NASH; however, in isolated cholangiocytes, inhibition of p16 decreased FOXO1 expression. FOXO1 regulates metabolic homeostasis, thus making FOXO1 an important target of NAFLD (43). The link between p16 and FOXO1 via E2F1 was confirmed in our study. E2F1 increased in human NAFLD/NASH that was inhibited by p16 VM. E2F1 has been identified as a mediator of glycolysis and lipogenesis (44). E2F1 increased in isolated cholangiocytes from human NAFLD/NASH compared to controls, but decreased with p16 VM. In support of this, E2F1 expression increases in liver biopsies from obese, glucose-intolerant humans compared with lean patient biopsies (44). Further, hepatocytes from *E2F1*$^{+/+}$ mice displayed increased glycolytic and lipogenic genes (44); however, no prior studies have demonstrated the contribution of biliary E2F1. Our previous work demonstrated that MCs can be recruited to the liver during NAFLD via IGF-1 signaling and the inhibition of IGF-1, *in vitro*, decreased MC migration (13). We examined *IGF-1* expression and found increased *IGF-1* in isolated cholangiocytes that decreases with p16 VM treatment in both WT HFD mice and human NAFLD/NASH. While our current studies demonstrate that p16 regulates IGF-1, others found that IGF-1 may mediate cellular senescence. For example, a specific IGF binding protein, IGFBP5, induced human umbilical endothelial cell senescence (45) demonstrating a feedback mechanism between IGF-1 and cellular senescence. While p16 VM did not alter the mRNA stability of *E2f1 or* ubiquitination of E2F1, p16 significantly reduced the transcription initiation process of *E2f1* and p16 VM reduced E2F1-facilitated transcription of *Foxo1*.

Adipose tissue maintains overall energy homeostasis through fat storage (46), and during NAFLD, enhanced food intake increases hepatic steatosis and visceral adiposity. SASP factors from senescent preadipocytes cause inflammation and macrophage infiltration in adipose tissue (47). Inhibition of senescence by removal of p16-positive adipocytes restored adipogenesis by upregulation of peroxisome proliferator-activated receptor-γ (PPARγ), carbohydrate element receptor binding protein alpha (C/EBPα) levels and subcutaneous adipose tissue expansion in obese mice, but interestingly decreased visceral adipocyte size (48). Our data demonstrate that p16 VM reduced key enzymes responsible for *de novo* synthesis and uptake of triglycerides and suggests inhibition of senescence alters the adaptive response due to nutritional abundance in our HFD fed NAFLD model. Lastly, we recognize that p16 is a tumor suppressor; however, the cell cycle is regulated by several

other tumor suppressor proteins. Suppression of p16 expression by oligonucleotide-based translational blocking would not affect the transcription and p16 protein levels would return to normal following degradation of p16 VM. Further, the dosage used *in vivo* did not trigger any counterintuitive effects such as tumorigenesis and the rescue of *Cdk4* and *Ccnd1* gene expression in WT HFD p16 VM mice did not surpass the CD-fed groups. Therefore, we propose the concept that transient suppression of p16 has potential therapeutic benefits in NAFLD/NASH without jeopardizing cell division.

Supplementary Material

Refer to Web version on PubMed Central for supplementary material.

Acknowledgements:

We are grateful to Dr. Thomas M. O'Connell, Center for Cachexia Research Innovation and Therapy for assistance with metabolomic studies including Biocrates plate run and analysis. We thank Mr, Aditya Sheth, Department of Pediatrics, Indiana University School of Medicine for assistance with the Deltavision Ultra microscope and Imaris image analysis software.

This work was supported by the Hickam Endowed Chair, Gastroenterology, Medicine, Indiana University, the Indiana University Health - Indiana University School of Medicine Strategic Research Initiative, the Senior Career Scientist Award (IK6 BX004601) and the VA Merit award (5I01BX000574) to GA and the Career Scientist Award (IK6BX005226) and the VA Merit award (1I01BX003031) to HF, and Career Development Award-2 to LK (1IK2BX005306) from the United States Department of Veteran's Affairs, Biomedical Laboratory Research and Development Service and NIH grants DK108959 and DK119421 (HF), DK054811, DK115184, DK076898, DK107310, DK110035, DK062975 and AA028711 (GA and SG) and the PSC Partners Seeking a Cure (GA). EG and PO were supported by research funds from Sapienza University of Rome. Portions of these studies were supported by resources at the Richard L. Roudebush VA Medical Center, Indianapolis, IN, and Medical Physiology, Medical Research Building, Temple, TX. The views expressed in this article are those of the authors and do not necessarily represent the views of the Department of Veterans Affairs.

Abbreviations:

ALT	Alanine aminotransferase
AST	aspartate transaminase
CD	control diet
CD-68	cluster of differentiation 68
CDK4	cyclin dependent kinase 4
Cer	Ceramide
ChIP-PCR	chromatin immunoprecipitation polymerase chain reaction
Co-IP	co-immunoprecipitation
CK-19	cytokeratin 19
CPT1A	carnitine palmitoyl transferase 1A
CPT1B	carnitine palmitoyl transferase 1B
DR	ductular reaction

DGAT2	diacyl glycerol acyl transferase 2
DMSO	Dimethyl Sulfoxide
E2F1	E2 promoter binding transcription factor 1
EIA	enzyme linked immunoassay
FABP1	fatty acid binding protein 1
FCεR1γ	FC epsilon receptor 1 gamma
FFA	free fatty acid
FITC	fluorescein isothiocyanate
FOXO1	Fork-head box transcription factor 1
GAPDH	glyceraldehyde 3 phosphate dehydrogenase
γH2A.X	phosphorylated histone 2A
GPAT3	glyceraldehyde 3 phosphate acyl transferase 3
HFD	high fat diet
H&E	hematoxylin and eosin
HNF4α	hepatocyte nuclear factor 4 alpha
HPC	hepatic progenitor cells
HSC	hepatic stellate cell
IBDM	intrahepatic bile duct mass
IF	immunofluorescence
IGF-1	insulin-like growth factor-1
IGFBP5	insulin like growth factor binding protein 5
IGF1R	insulin like growth factor 1 receptor
IL-6	interleukin-6
IMCL	immortalized murine cholangiocyte cell line
KO	knockout
LW/BW	liver weight/ body weight
MC	mast cell
MCD	methionine-choline deficient

Mdr2 $^{-/-}$	multidrug resistance transporter 2/ ABC transporter B family member 2 knock out
miR/miRNA	micro ribonucleic acid
NAFLD	non-alcoholic fatty liver disease
NASH	non-alcoholic steatohepatitis
OA	oleic acid/oleate
PA	palmitic acid/palmitate
p16	cyclin-dependent kinase inhibitor 2A
p18	cyclin-dependent kinase 4 inhibitor C
p21	cyclin-dependent kinase inhibitor 1A
PBS	phosphate buffered saline
PSC	primary sclerosing cholangitis
***q*PCR**	quantitative polymerase chain reaction
RNA pol II	RNA polymerase II
Rpb1 NTD	RNA polymerase II subunit 1 N-terminal domain
Rps18	mouse ribosomal protein s18
SA	stearic acid/stearate
SASPs	senescence associated secretory phenotypes
TGF-β1	transforming growth factor beta 1
SIRT1	sirtuin1
TPSβ2	tryptase β2
TUNEL	Terminal deoxynucleotidyl transferase dUTP nick end labeling
VM	vivo morpholino
WB	western blot
WT	wild type

References

1. Pierantonelli I, Svegliati-Baroni G. Nonalcoholic Fatty Liver Disease: Basic Pathogenetic Mechanisms in the Progression From NAFLD to NASH. Transplantation 2019;103:e1–e13. [PubMed: 30300287]

2. Loomba R, Wong R, Fraysse J, Shreay S, Li S, Harrison S, Gordon SC. Nonalcoholic fatty liver disease progression rates to cirrhosis and progression of cirrhosis to decompensation and mortality: a real world analysis of Medicare data. Aliment Pharmacol Ther 2020;51:1149–1159. [PubMed: 32372515]

3. Dong XC. FOXO transcription factors in non-alcoholic fatty liver disease. Liver Res 2017;1:168–173. [PubMed: 30034912]

4. Zhang X, Xu GB, Zhou D, Pan YX. High-fat diet modifies expression of hepatic cellular senescence gene p16(INK4a) through chromatin modifications in adult male rats. Genes Nutr 2018;13:6. [PubMed: 29564021]

5. Sato K, Marzioni M, Meng F, Francis H, Glaser S, Alpini G. Ductular Reaction in Liver Diseases: Pathological Mechanisms and Translational Significances. Hepatology 2019;69:420–430. [PubMed: 30070383]

6. Tabibian JH, O'Hara SP, Splinter PL, Trussoni CE, LaRusso NF. Cholangiocyte senescence by way of N-ras activation is a characteristic of primary sclerosing cholangitis. Hepatology 2014;59:2263–2275. [PubMed: 24390753]

7. Chen L, Wu N, Kennedy L, Francis H, Ceci L, Zhou T, Samala N, et al. Inhibition of Secretin/Secretin Receptor Axis Ameliorates NAFLD Phenotypes. Hepatology 2021;74:1845–1863. [PubMed: 33928675]

8. Kyritsi K, Francis H, Zhou T, Ceci L, Wu N, Yang Z, Meng F, et al. Downregulation of p16 Decreases Biliary Damage and Liver Fibrosis in the Mdr2(/) Mouse Model of Primary Sclerosing Cholangitis. Gene Expr 2020;20:89–103. [PubMed: 32393417]

9. Kennedy L, Hargrove L, Demieville J, Bailey JM, Dar W, Polireddy K, Chen Q, et al. Knockout of l-Histidine Decarboxylase Prevents Cholangiocyte Damage and Hepatic Fibrosis in Mice Subjected to High-Fat Diet Feeding via Disrupted Histamine/Leptin Signaling. Am J Pathol 2018;188:600–615. [PubMed: 29248461]

10. Petrescu AD, Grant S, Williams E, Frampton G, Reinhart EH, Nguyen A, An S, et al. Ghrelin reverses ductular reaction and hepatic fibrosis in a rodent model of cholestasis. Sci Rep 2020;10:16024. [PubMed: 32994489]

11. Zhang L, Zhang Z, Li C, Zhu T, Gao J, Zhou H, Zheng Y, et al. S100A11 Promotes Liver Steatosis via FOXO1-Mediated Autophagy and Lipogenesis. Cell Mol Gastroenterol Hepatol 2021;11:697–724. [PubMed: 33075563]

12. Kamagate A, Qu S, Perdomo G, Su D, Kim DH, Slusher S, Meseck M, et al. FoxO1 mediates insulin-dependent regulation of hepatic VLDL production in mice. J Clin Invest 2008;118:2347–2364. [PubMed: 18497885]

13. Kennedy L, Meadows V, Sybenga A, Demieville J, Chen L, Hargrove L, Ekser B, et al. Mast Cells Promote Nonalcoholic Fatty Liver Disease Phenotypes and Microvesicular Steatosis in Mice Fed a Western Diet. Hepatology 2021;74:164–182. [PubMed: 33434322]

14. Pi H, Liu M, Xi Y, Chen M, Tian L, Xie J, Chen M, et al. Long-term exercise prevents hepatic steatosis: a novel role of FABP1 in regulation of autophagy-lysosomal machinery. FASEB J 2019;33:11870–11883. [PubMed: 31366243]

15. Tang M, Dong X, Xiao L, Tan Z, Luo X, Yang L, Li W, et al. CPT1A-mediated fatty acid oxidation promotes cell proliferation via nucleoside metabolism in nasopharyngeal carcinoma. Cell Death Dis 2022;13:331. [PubMed: 35411000]

16. Kennedy LL, Hargrove LA, Graf AB, Francis TC, Hodges KM, Nguyen QP, Ueno Y, et al. Inhibition of mast cell-derived histamine secretion by cromolyn sodium treatment decreases biliary hyperplasia in cholestatic rodents. Lab Invest 2014;94:1406–1418. [PubMed: 25365204]

17. Meadows V, Kennedy L, Ekser B, Kyritsi K, Kundu D, Zhou T, Chen L, et al. Mast Cells Regulate Ductular Reaction and Intestinal Inflammation in Cholestasis Through Farnesoid X Receptor Signaling. Hepatology 2021;74:2684–2698. [PubMed: 34164827]

18. Bernadotte A, Mikhelson VM, Spivak IM. Markers of cellular senescence. Telomere shortening as a marker of cellular senescence. Aging (Albany NY) 2016;8:3–11. [PubMed: 26805432]

19. Rockey DC, Du Q, Weymouth ND, Shi Z. Smooth Muscle alpha-Actin Deficiency Leads to Decreased Liver Fibrosis via Impaired Cytoskeletal Signaling in Hepatic Stellate Cells. Am J Pathol 2019;189:2209–2220. [PubMed: 31476284]

20. Masoodi M, Gastaldelli A, Hyotylainen T, Arretxe E, Alonso C, Gaggini M, Brosnan J, et al. Metabolomics and lipidomics in NAFLD: biomarkers and non-invasive diagnostic tests. Nat Rev Gastroenterol Hepatol 2021.
21. Al-Khalaf HH, Colak D, Al-Saif M, Al-Bakheet A, Hendrayani SF, Al-Yousef N, Kaya N, et al. p16(INK4a) positively regulates cyclin D1 and E2F1 through negative control of AUF1. PLoS One 2011;6:e21111. [PubMed: 21799732]
22. Eymin B, Karayan L, Seite P, Brambilla C, Brambilla E, Larsen CJ, Gazzeri S. Human ARF binds E2F1 and inhibits its transcriptional activity. Oncogene 2001;20:1033–1041. [PubMed: 11314038]
23. Mason SL, Loughran O, La Thangue NB. p14(ARF) regulates E2F activity. Oncogene 2002;21:4220–4230. [PubMed: 12082609]
24. Inoue T, Plieth D, Venkov CD, Xu C, Neilson EG. Antibodies against macrophages that overlap in specificity with fibroblasts. Kidney Int 2005;67:2488–2493. [PubMed: 15882296]
25. Alsuraih M, O'Hara SP, Woodrum JE, Pirius NE, LaRusso NF. Genetic or pharmacological reduction of cholangiocyte senescence improves inflammation and fibrosis in the Mdr2 (−/−) mouse. JHEP Rep 2021;3:100250.
26. Cazzagon N, Sarcognato S, Floreani A, Corra G, De Martin S, Guzzardo V, Russo FP, et al. Cholangiocyte senescence in primary sclerosing cholangitis is associated with disease severity and prognosis. JHEP Rep 2021;3:100286.
27. Lv F, Wu J, Miao D, An W, Wang Y. p16 deficiency promotes nonalcoholic steatohepatitis via regulation of hepatic oxidative stress. Biochem Biophys Res Commun 2017;486:264–269. [PubMed: 28286271]
28. Ogrodnik M, Miwa S, Tchkonia T, Tiniakos D, Wilson CL, Lahat A, Day CP, et al. Cellular senescence drives age-dependent hepatic steatosis. Nat Commun 2017;8:15691. [PubMed: 28608850]
29. Passos JF, Nelson G, Wang C, Richter T, Simillion C, Proctor CJ, Miwa S, et al. Feedback between p21 and reactive oxygen production is necessary for cell senescence. Mol Syst Biol 2010;6:347. [PubMed: 20160708]
30. Lv F, Li N, Kong M, Wu J, Fan Z, Miao D, Xu Y, et al. CDKN2a/p16 Antagonizes Hepatic Stellate Cell Activation and Liver Fibrosis by Modulating ROS Levels. Front Cell Dev Biol 2020;8:176.
31. Chiba M, Sasaki M, Kitamura S, Ikeda H, Sato Y, Nakanuma Y. Participation of bile ductular cells in the pathological progression of non-alcoholic fatty liver disease. J Clin Pathol 2011;64:564–570. [PubMed: 21486894]
32. Nobili V, Carpino G, Alisi A, Franchitto A, Alpini G, De Vito R, Onori P, et al. Hepatic progenitor cells activation, fibrosis, and adipokines production in pediatric nonalcoholic fatty liver disease. Hepatology 2012;56:2142–2153. [PubMed: 22467277]
33. Carpino G, Pastori D, Baratta F, Overi D, Labbadia G, Polimeni L, Di Costanzo A, et al. PNPLA3 variant and portal/periportal histological pattern in patients with biopsy-proven non-alcoholic fatty liver disease: a possible role for oxidative stress. Sci Rep 2017;7:15756. [PubMed: 29150621]
34. Carpino G, Nobili V, Renzi A, De Stefanis C, Stronati L, Franchitto A, Alisi A, et al. Macrophage Activation in Pediatric Nonalcoholic Fatty Liver Disease (NAFLD) Correlates with Hepatic Progenitor Cell Response via Wnt3a Pathway. PLoS One 2016;11:e0157246.
35. Nobili V, Carpino G, De Peppo F, Caccamo R, Mosca A, Romito I, Overi D, et al. Laparoscopic Sleeve Gastrectomy Improves Nonalcoholic Fatty Liver Disease-Related Liver Damage in Adolescents by Reshaping Cellular Interactions and Hepatic Adipocytokine Production. J Pediatr 2018;194:100–108 e103. [PubMed: 29198531]
36. Pirola CJ, Sookoian S. Multiomics biomarkers for the prediction of nonalcoholic fatty liver disease severity. World J Gastroenterol 2018;24:1601–1615. [PubMed: 29686467]
37. Enooku K, Nakagawa H, Fujiwara N, Kondo M, Minami T, Hoshida Y, Shibahara J, et al. Altered serum acylcarnitine profile is associated with the status of nonalcoholic fatty liver disease (NAFLD) and NAFLD-related hepatocellular carcinoma. Sci Rep 2019;9:10663. [PubMed: 31337855]
38. Oxenkrug GF. Metabolic syndrome, age-associated neuroendocrine disorders, and dysregulation of tryptophan-kynurenine metabolism. Ann N Y Acad Sci 2010;1199:1–14. [PubMed: 20633104]

39. Zhang A, Carroll C, Raigani S, Karimian N, Huang V, Nagpal S, Beijert I, et al. Tryptophan Metabolism via the Kynurenine Pathway: Implications for Graft Optimization during Machine Perfusion. J Clin Med 2020;9.
40. Piras C, Noto A, Ibba L, Deidda M, Fanos V, Muntoni S, Leoni VP, et al. Contribution of Metabolomics to the Understanding of NAFLD and NASH Syndromes: A Systematic Review. Metabolites 2021;11.
41. Georgin-Lavialle S, Launay JM, Cote F, Soucie E, Soria A, Damaj G, Moura DS, et al. Decreased tryptophan and increased kynurenine levels in mastocytosis associated with digestive symptoms. Allergy 2016;71:416–420. [PubMed: 26841279]
42. Valenti L, Rametta R, Dongiovanni P, Maggioni M, Fracanzani AL, Zappa M, Lattuada E, et al. Increased expression and activity of the transcription factor FOXO1 in nonalcoholic steatohepatitis. Diabetes 2008;57:1355–1362. [PubMed: 18316359]
43. Kousteni S. FoxO1: a molecule for all seasons. J Bone Miner Res 2011;26:912–917. [PubMed: 21541992]
44. Denechaud PD, Lopez-Mejia IC, Giralt A, Lai Q, Blanchet E, Delacuisine B, Nicolay BN, et al. E2F1 mediates sustained lipogenesis and contributes to hepatic steatosis. J Clin Invest 2016;126:137–150. [PubMed: 26619117]
45. Kim KS, Seu YB, Baek SH, Kim MJ, Kim KJ, Kim JH, Kim JR. Induction of cellular senescence by insulin-like growth factor binding protein-5 through a p53-dependent mechanism. Mol Biol Cell 2007;18:4543–4552. [PubMed: 17804819]
46. Mau T, Yung R. Adipose tissue inflammation in aging. Exp Gerontol 2018;105:27–31. [PubMed: 29054535]
47. Xu M, Tchkonia T, Ding H, Ogrodnik M, Lubbers ER, Pirtskhalava T, White TA, et al. JAK inhibition alleviates the cellular senescence-associated secretory phenotype and frailty in old age. Proc Natl Acad Sci U S A 2015;112:E6301–6310. [PubMed: 26578790]
48. Palmer AK, Xu M, Zhu Y, Pirtskhalava T, Weivoda MM, Hachfeld CM, Prata LG, et al. Targeting senescent cells alleviates obesity-induced metabolic dysfunction. Aging Cell 2019;18:e12950. [PubMed: 30907060]

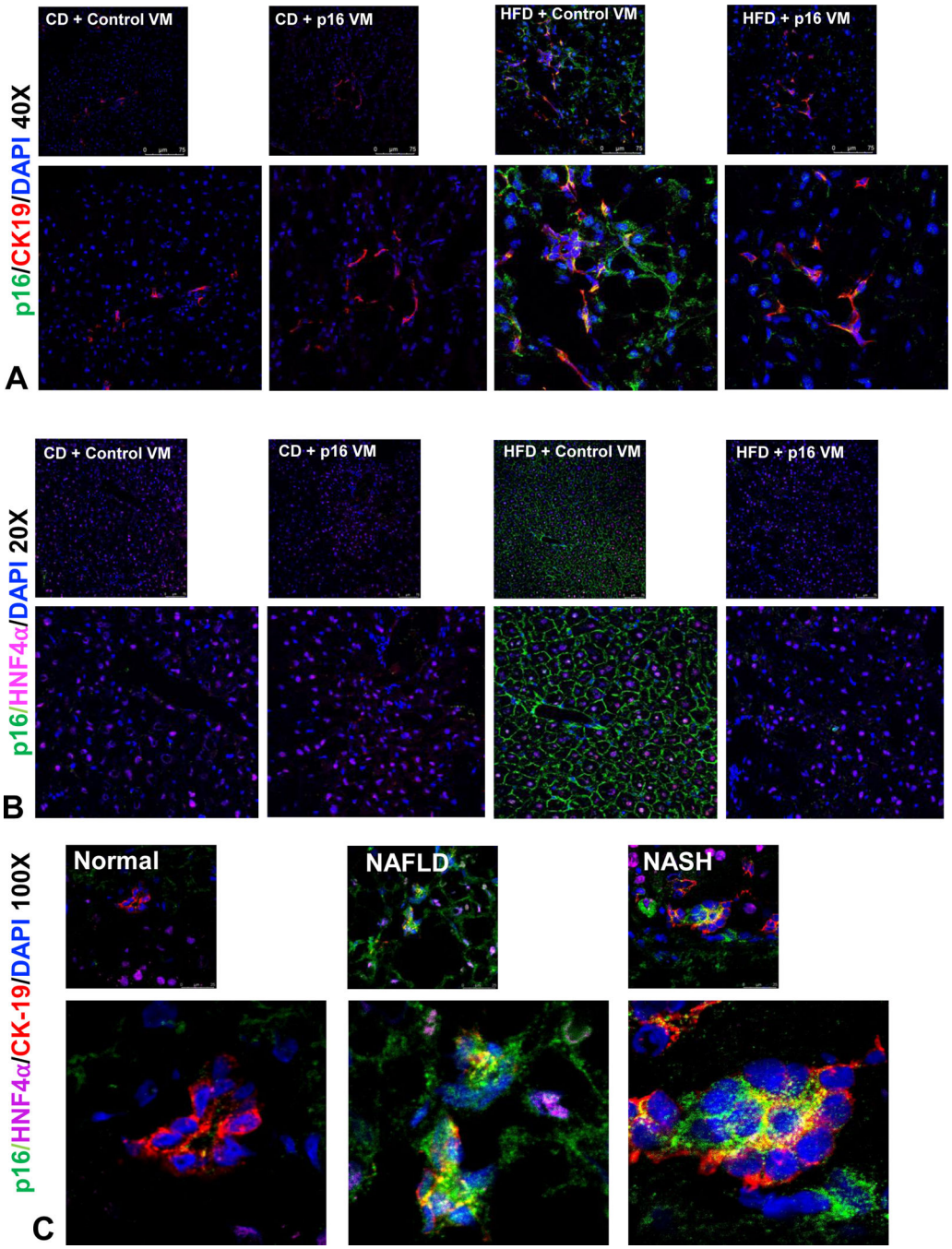

Figure 1: p16 expression is reduced in HFD fed mice after treatment with p16 VM.

WT HFD fed mice injected with control VM showed a robust increase in p16 immunoreactivity (green) in cholangiocytes (red, **A**) and in hepatocytes (magenta, **B**). p16 VM injection in HFD mice reduced p16 immunostaining in both cholangiocytes (**A**) and hepatocytes (**B**). There were visible differences between the CD control VM and p16 VM injected groups. In human NAFLD and NASH, p16 immunoreactivity (p16, green) increased in both cholangiocytes (red) and hepatocytes (magenta) compared to normal control (**C**).

Representative images from n = 4 are shown at 40x and 20x, respectively for the mouse and 100x for human staining (n = 4).

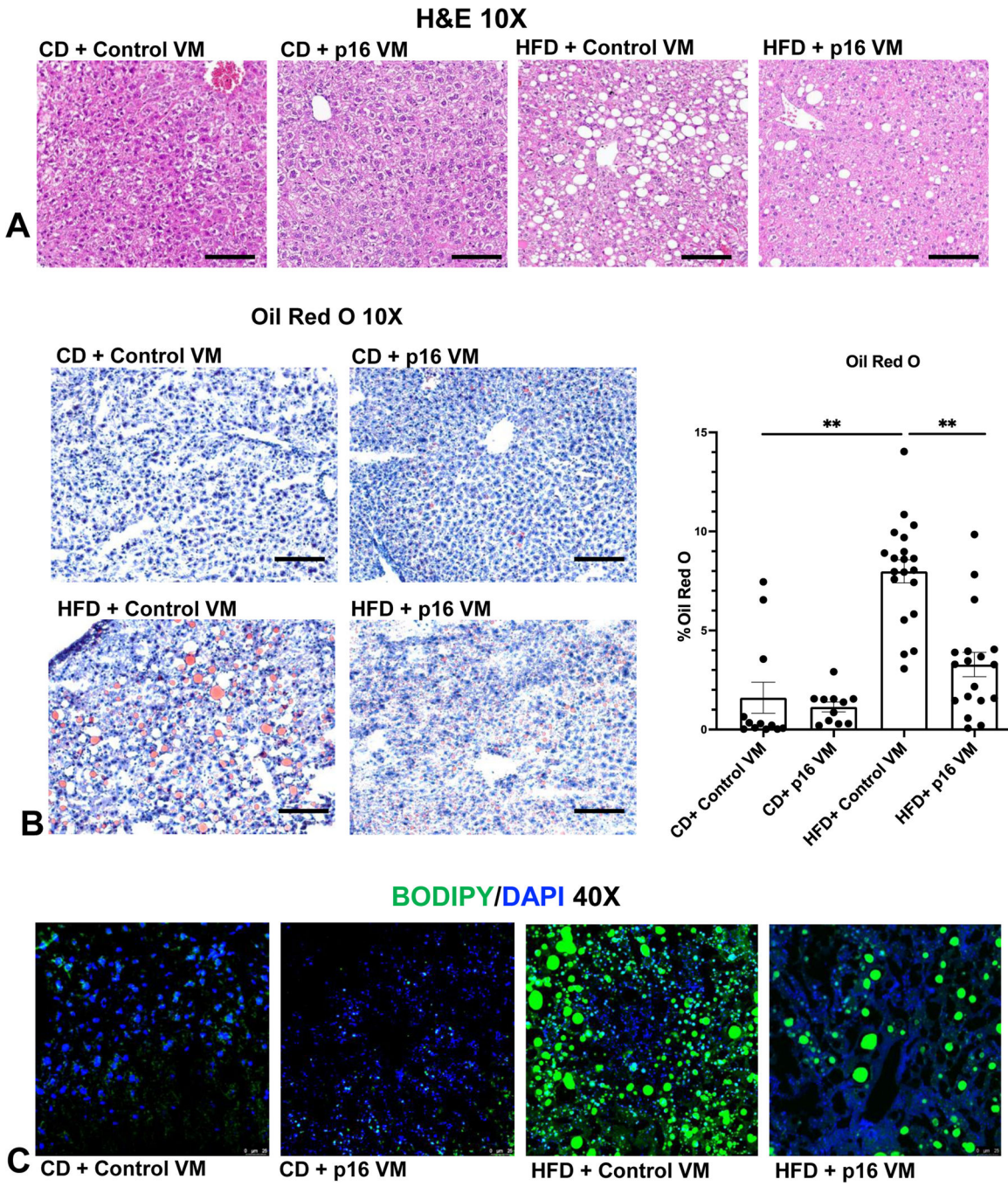

Figure 2: p16 VM reduced steatosis in WT HFD fed mice.

By H&E staining we found that WT HFD mice had moderate steatosis with stage 1–2 portal fibrosis, ballooning hepatocytes, inflammation, and ductular proliferation compared to CD fed mice treated with control VM. Treatment with p16 VM in WT HFD fed mice displayed patchy ductular proliferation and steatosis, the absence of ballooning hepatocytes and minimal stage 1–2 fibrosis as shown by H&E (10x); there were no noticeable differences between the CD control VM and CD p16 VM mice (**A**). Oil Red O staining (10x) showed a significant increase in % lipid droplet area (steatosis) in HFD control VM mice compared

to CD control VM mice and WT HFD mice treated with p16 VM had a significant reduction in lipid droplet presence (**B**). BODIPY staining (40x) demonstrated increased neutral lipid droplet presence in WT HFD control VM mice compared to CD control VM which decreased in HFD p16 VM mice (**C**). Data are expressed as mean ± SEM. Each dot represents an image; n = 12–20 images from n = 4–6 mice for Oil Red O were used for semi-quantification. Representative images for stains were chosen from n = 12–20 images per group for (**B**). ***P<0.05.*

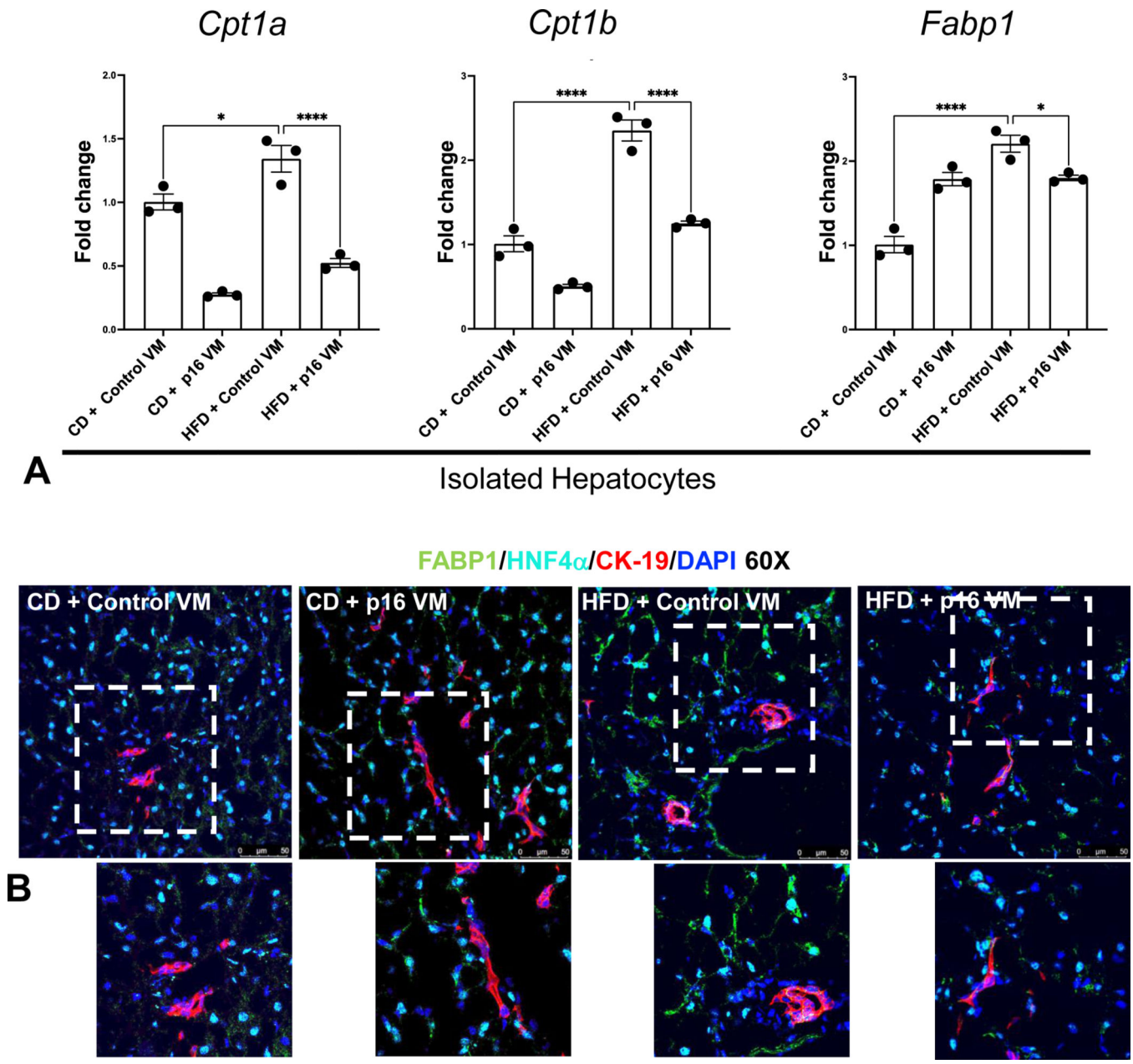

Figure 3: p16 VM reduces lipid transport and oxidation in hepatocytes in WT HFD fed mice.

Fatty acid uptake and oxidation gene expression of *Cpt1a, Cpt1b,* and *Fabp1* was significantly upregulated in hepatocytes isolated from WT HFD control VM compared to CD control VM mice. Hepatocytes isolated from HFD p16 VM mice had significantly reduced expression of these genes compared to HFD control group (**A**). Immunoreactivity of FABP1 (green) in hepatocytes stained with HNF4α (cyan) increased in WT HFD control VM mice compared to the CD control VM; however, WT HFD p16 VM mice showed a marked reduction in FABP1 immunoreactivity compared to HFD control VM mice. Cholangiocytes (red) did not show any marked immunostaining of FABP1 (**B**). Data are expressed as mean fold change ± SEM. Each dot of *q*PCR represents a technical replicate from hepatocytes of n = 4–6 mice for *q*PCR and normalized with *Gapdh* as the

housekeeping gene. FABP1 immunostaining (60x) and are representative of liver sections from at least 4 different animals per group. *****P< 0.001; *P< 0.05.*

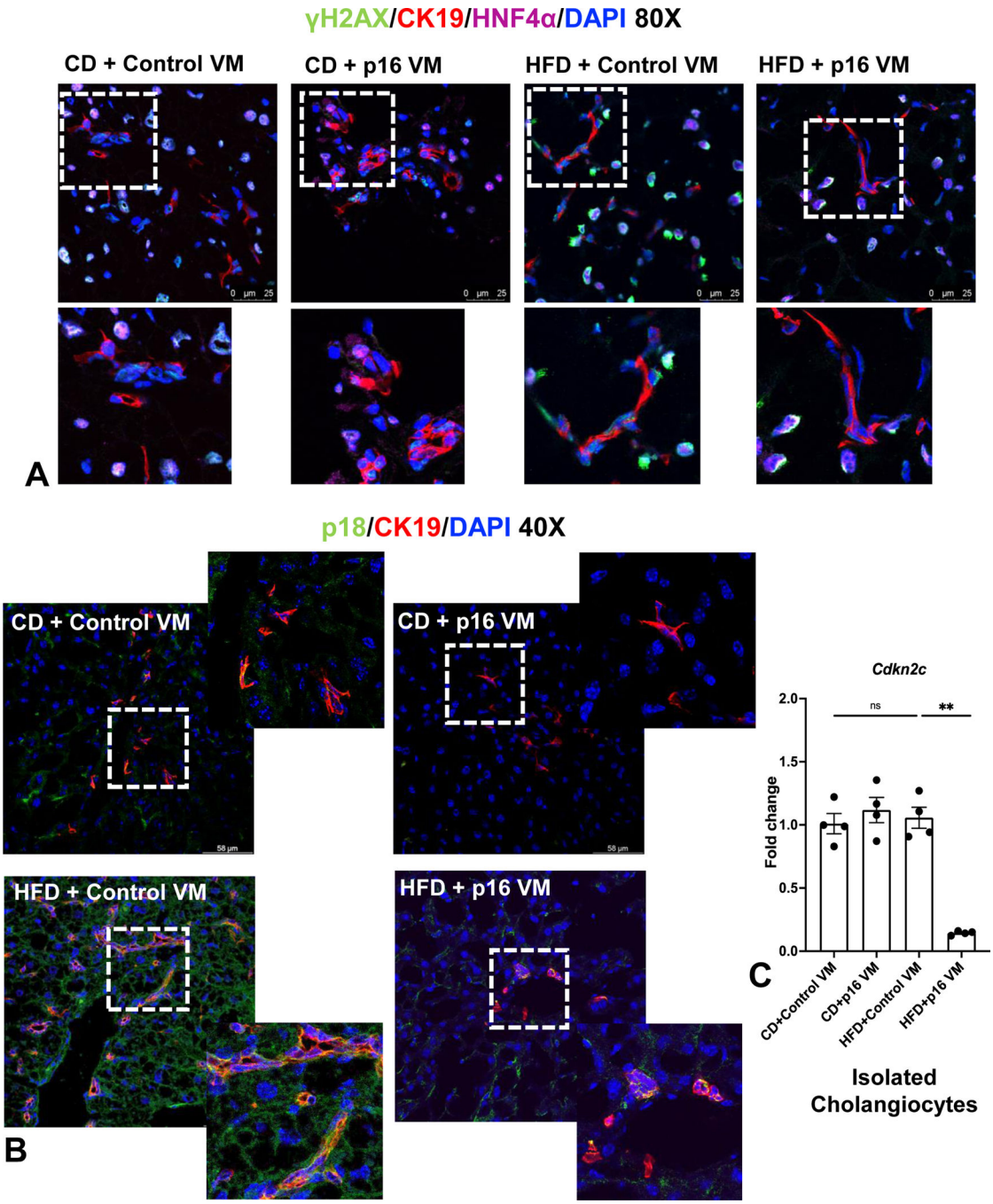

Figure 4: p16 VM reduced hepatocyte and cholangiocyte senescence in WT HFD fed mice.

γH2A.X (green) staining was elevated in both hepatocytes (cyan) and cholangiocytes (red) of HFD control VM mice and HFD p16 VM mice had reduced γH2A.X staining in both cholangiocytes and hepatocytes (**A**). p18 immunostaining (co-stained with CK-19) increased in HFD control VM mice compared to CD control VM and when p16 VM was administered to HFD mice, p18 expression decreased (**B**). By *q*PCR, gene expression of p18 (*Cdkn2c*) did not change between WT CD control or p16 VM or WT HFD control VM; however, there was significant reduction of p18 expression in WT HFD mice treated with p16 VM

(**C**). Data are expressed as mean ± SEM. Each dot of *q*PCR represents a technical replicate of 4 reactions from n = 4–6 mice and normalized with *Rps18* as the housekeeping gene. Immunostaining of γH2A.X (80x) and p18 (40x) are representative of at least 4 different sections of tissues per treatment group. ***P< 0.001; ns = non-significant*.

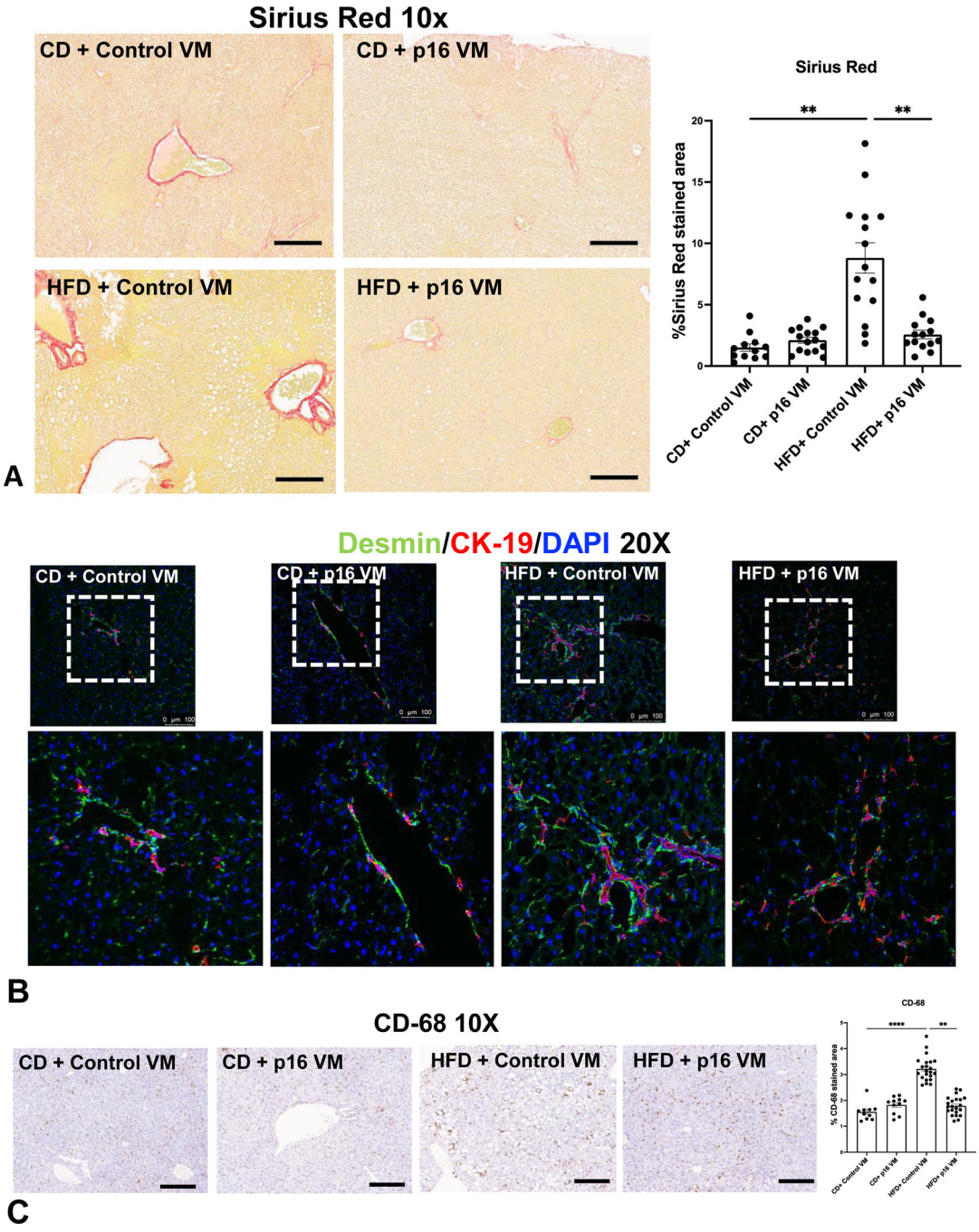

Figure 5: p16 VM treatment reduced collagen deposition, HSC activation and inflammation in WT HFD mice.

WT HFD control VM mice displayed a significant increase in Sirius Red staining/collagen deposition compared to WT CD control VM mice, which was significantly reduced in WT HFD p16 VM mice (**A**). Co-immunostaining of desmin (green) with CK-19 (red) indicated increased immunoreactivity of desmin (20x) in the portal area in WT HFD control VM mice compared to CD control VM mice, whereas p16 VM treatment decreased desmin immunoreactivity in WT HFD fed mice (**B**). CD-68 positivity significantly increased in

WT HFD control VM mice compared to CD control VM mice and CD-68 positive cells significantly decreased in WT HFD p16 VM mice (**C**). Data are expressed as mean ± SEM. Each dot represents an image; n = 12–15 images from n = 4–6 mice were used for Sirius Red (10x) and n = 10–20 images for CD-68 (10x) semi-quantification. Representative images of desmin/CK-19 staining were obtained from at least n = 6 images per group. *****P< 0.001; ** P< 0.05.*

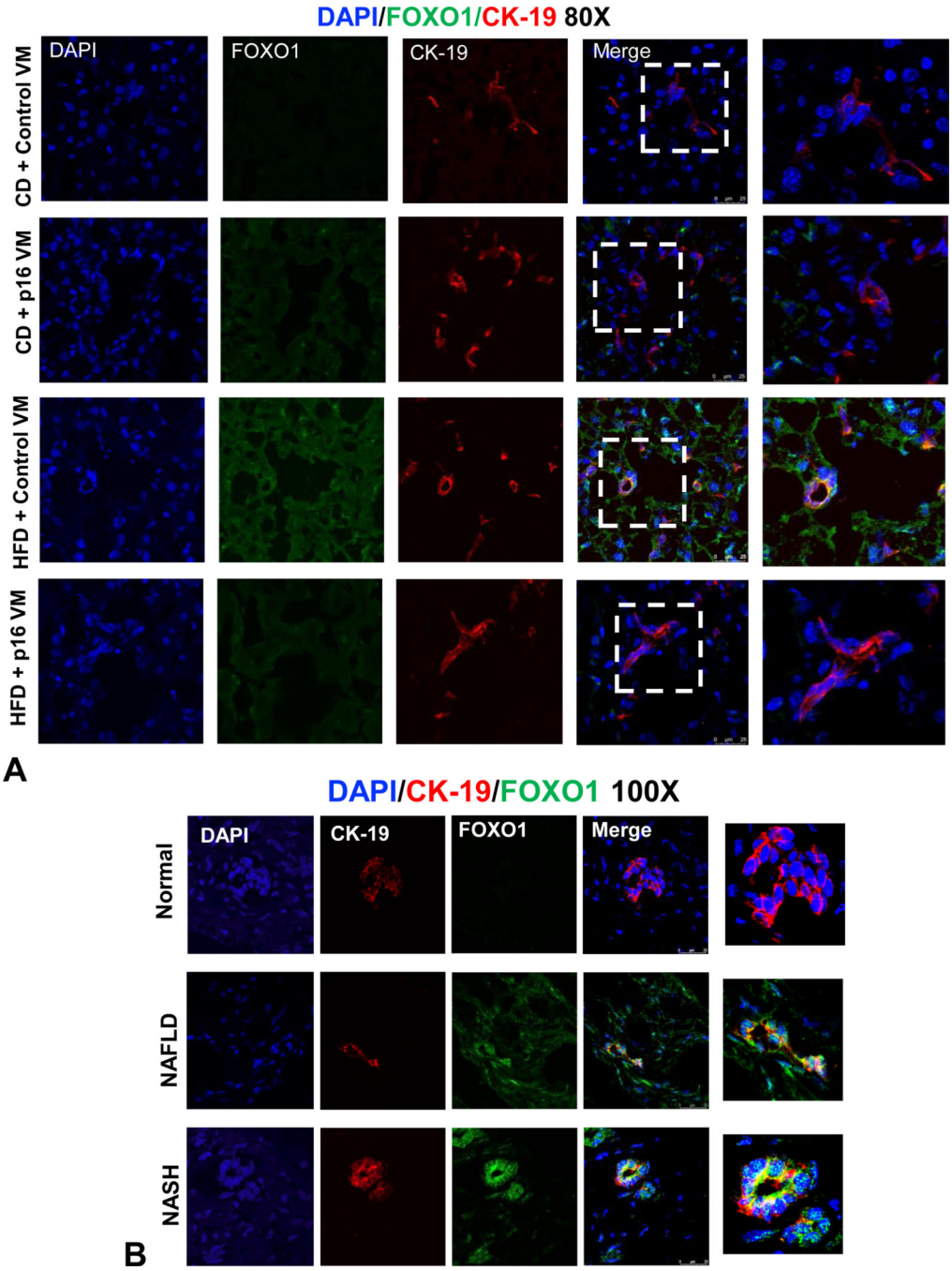

Figure 6: p16 regulation of biliary FOXO1 expression in WT mice fed with HFD and in human NAFLD/NASH patients.

FOXO1 immunostaining (green) increased in cholangiocytes (red) in WT HFD mice treated with control VM compared to CD control VM mice and FOXO1 immunoreactivity decreased in WT HFD mice treated with p16 VM compared to the control (**A**). FOXO1 (green) immunoreactivity was enhanced in cholangiocytes (red) of NAFLD, and NASH patients compared to the normal controls **(B).** Representative images for FOXO1/CK-19

staining for **(A)** were obtained from at least n = 6 images per group at 80 x magnification and 100x magnification for (**B**) representative of n = 4 for each group.

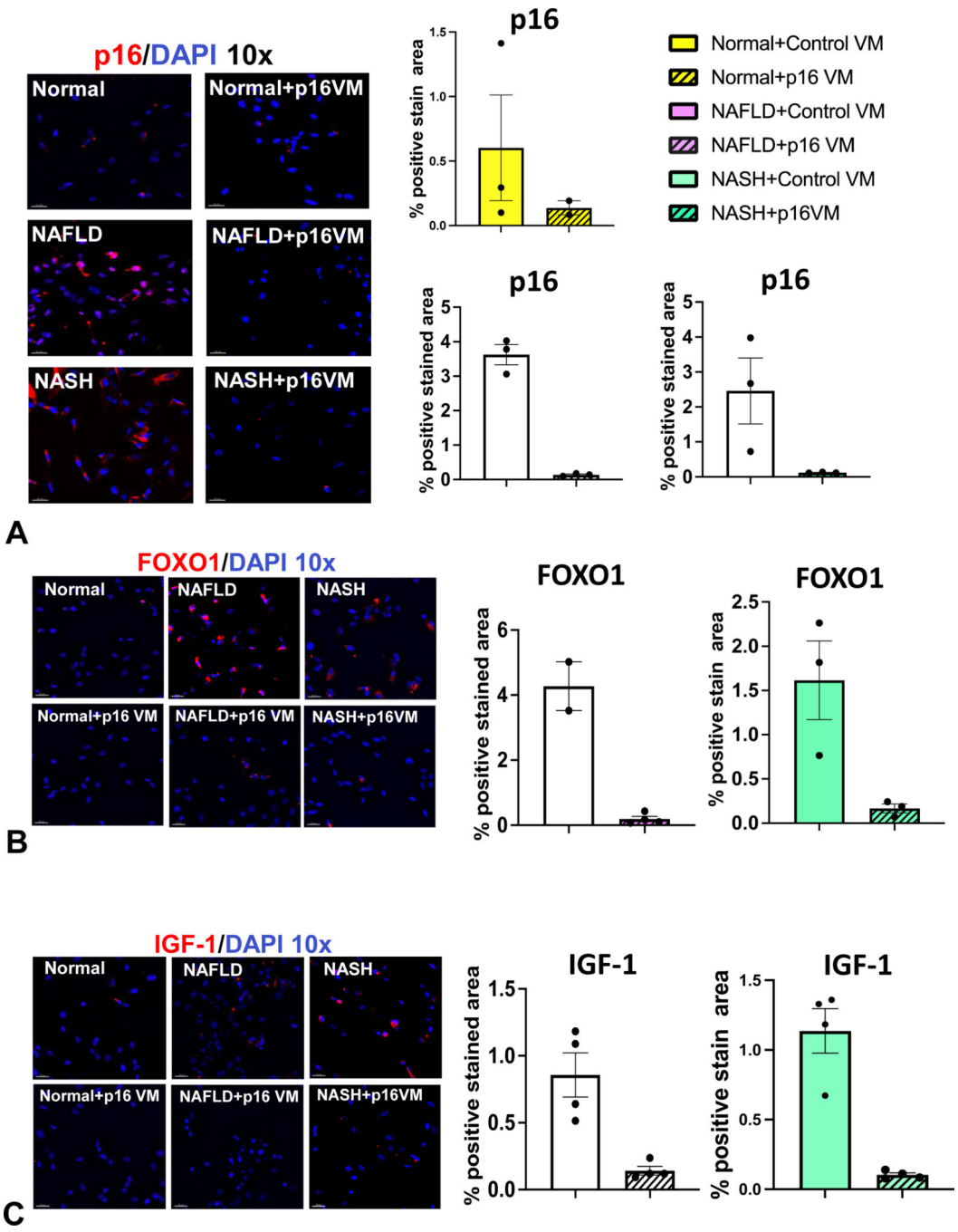

Figure 7: p16 regulation of biliary FOXO1/IGF-1 signaling in human NAFLD/NASH.

In isolated human cholangiocytes from NAFLD and NASH patients, p16 immunoreactivity increased compared to normal human cholangiocytes and when isolated NAFLD/NASH cholangiocytes were treated with p16 VM, p16 immunoreactivity decreased compared to the control VM treated cells (**A**). By immunofluorescence, we found that biliary FOXO1(**B**) and IGF-1 (**C**) immunoreactivity increased in liver samples from NAFLD/NASH compared to respective control groups. Each dot represents an image. Semi-quantification of immunofluorescence staining is expressed as mean ± SEM from at least 2 non-overlapping

images taken at 10x magnification. Representative images of human liver sections are from n = 4 patient per group at 100x magnification.

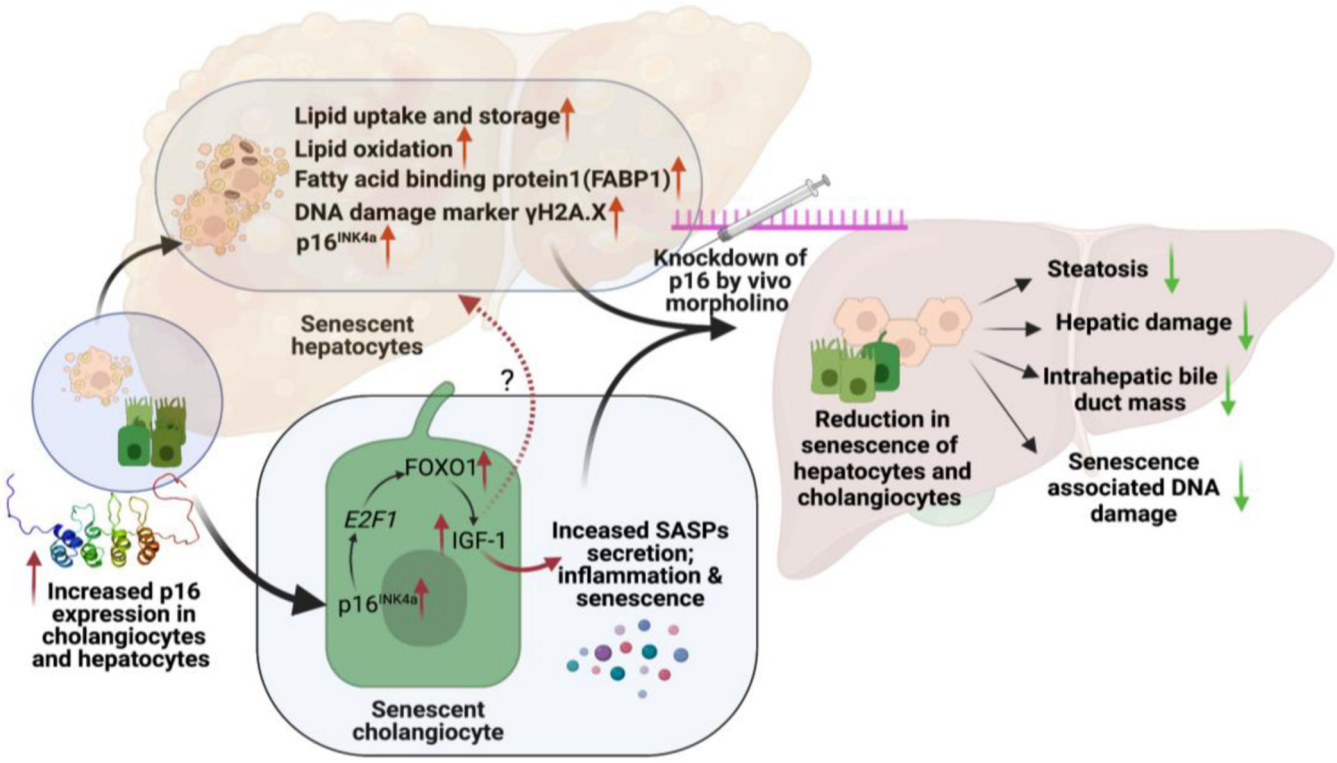

Figure 8: Working Model:

p16 expression in cholangiocytes and hepatocytes increases following HFD. Increased p16 in hepatocytes results in elevated uptake of long chain fatty acids via FABP1 and increased fat oxidation. Increased p16 in cholangiocytes results in elevated IGF-1 production via upregulation of the E2F1/FOXO1 axis. p16 VM injection reduces p16 expression in both hepatocytes and cholangiocytes leading to a marked reduction in NAFLD phenotypes and downregulation of E2F1/FOXO1/IGF-1 in cholangiocytes. *Image produced by* BioRender.com.

Table 1:

Liver weight/body weight ratio of mice across all groups

	n	Mean Liver Weight (g)	Mean Body Weight (g)	Mean LW/BW
CD+ Control VM	15	1.48 ±0.06	30.77 ± 1.07	4.84 ±0.16
CD+p16 VM	12	1.36 ± 0.05	31.79 ± 0.83	4.28 ± 0.14
HFD+ Control VM	14	2.83 ± 0.26**	34.64 ± 1.09	8.03 ± 0.51**
HFD+p16 VM	14	2.16 ± 0.13*	33.33 ± 0.74	6.47 ± 0.31*

Note: p16 VM treatment reduced LW, but did not significantly reduce BW; however, overall LW/BW ratio decreased significantly compared to HFD control VM group. Data represented as mean ± SEM.

** *P<0.*05 vs. CD Control VM

* *P<0.*05 vs. HFD control VM

Table 2:

Serum chemistry showing key biomarkers of liver damage

	AST (U/L)	ALT (U/L)	Total cholesterol (mg/dl)
CD + Control VM	72± 3.13	93± 0.57	151± 0
CD + p16 VM	88 ± 0.82	101.5± 0.28	166.25± 1.03
HFD + Control VM	212.25±2.28 **	196.5± 1.19 **	223± 1 **
HFD + p16 VM	198.5± 0.95 *	162± 1.15 *	190.25± 0.75 *

Note: p16 VM treatment significantly reduced serum levels of AST and ALT along with a reduction in total cholesterol compared to HFD control VM mice. Data represented as mean ± SEM.

** $P<0.05$ vs. CD Control VM

* $P<0.05$ vs. HFD control VM